Title

HIV causes global B-cell dysregulation and restricts HBV-specific B-cell development in an incident HBV cohort

Authors

Katherine Cascino[1]*, Thomas Liechti[2]*, Eric C. Seaberg[3], Kathleen Stevens[1], Steven M. Wolinsky[4], Mallory D. Witt[5], Robbie B. Mailliard[6], Mario Roederer[2], Justin Bailey[1], Chloe L Thio[1¥], Andrea Cox[1¥]

[1]Department of Medicine, Johns Hopkins University School of Medicine, Baltimore, Maryland, USA.

[2]ImmunoTechnology Section, Vaccine Research Center, NIAID, NIH, Bethesda, Maryland, USA.

[3]Department of Epidemiology, Johns Hopkins University, Baltimore, Maryland, USA.

[4]Division of Infectious Diseases, Department of Medicine, Feinberg School of Medicine, Northwestern University, Chicago, Illinois, USA.

[5]Lundquist Research Institute at Harbor-UCLA Medical Center, Torrance, CA, USA.

[6]Department of Medicine, University of Pittsburgh School of Medicine, Pittsburgh, Pennsylvania, USA.

TL's present address is: Section of Immunology, Division of Infection Control, Norwegian Institute of Public Health, Oslo, Norway.

*These authors contributed equally

¥Corresponding authors contributed equally: Chloe Thio, email: cthio@jhmi.edu; Andrea Cox, email: acox@jhmi.edu. 855 N. Wolfe Street, Rangos Building, Suite 520, Baltimore MD 21205. Phone: 410-502-3717.

The authors have declared that no conflict of interest exists.

Abstract

Background. Functional B cell responses for both prevention and control of hepatitis B virus (HBV) infection remain poorly understood, including in the context of HBV/HIV co-infection.

Methods. Here, we employed high-dimensional single cell analysis to assess global and hepatitis B surface antigen (HBsAg)-specific B cells in a longitudinal cohort of incident HBV from the Multicenter Aids Cohort Study (MACS), with a subset of the cohort living with HIV-1.

Results. We observed that prior HIV infection has negative consequences for B cell function in early post-acute HBV infection, including increased frequencies of atypical memory (AtM) B cells and regulatory B cells (B_{regs}), expression of the activation marker CD86 on multiple B cell subsets in chronic HBV (CHB), and restricted expansion of HBsAg-specific B cells. In contrast, in HBV mono-infection, we observed no changes in the global B cell population from prior to infection and robust expansion of HBsAg-specific B cells. These expanded antigen-specific B cells resembled class-switched intermediate and resting memory (IM and RM) B cells, with activation phenotypes that may contribute to ongoing HBV control.

Conclusion. HIV infection has a significant impact on B cell responses to subsequent HBV infection that may promote development of CHB in HBV/HIV co-infection.

Funding. National Institute of Allergy and Infectious Diseases, Bill & Melinda Gates Foundation.

Introduction

After infection with hepatitis B virus (HBV), 95% of immunocompetent adults control the infection and develop protective antibodies, whereas the remaining 5% develop chronic HBV (CHB), a leading cause of liver disease and hepatocellular carcinoma (HCC) globally. B lymphocytes play a crucial role in the prevention and control of HBV infection through diverse effector functions, including the secretion of antibodies and cytokines (1). Antibodies to the HBV surface antigen (anti-HBsAg) indicate control of an acute infection and protect against infection when generated through vaccination (2, 3). Further, B cell-depleting immunotherapy can lead to HBV reactivation even years after recovery from an acute infection, highlighting the importance of B cells in maintaining control (4–6). Thus, B cells are considered a target for generating a functional cure. However, there is a limited understanding of what constitutes an effective B cell response to HBV.

There is some evidence of perturbations in the global B cell population in CHB, including increased proportions of activated $CD69^{+}CD73^{+}$ B cells (7, 8) and atypical memory (AtM) B cells, a $CD21^{-}CD27^{-}$ B cell population often associated with chronic antigenic stimulation (9, 10). Expansion of these populations has negative consequences, including hyperactivation and functional impairment thought to contribute to poor viral clearance. Furthermore, B_{regs} emerge in CHB and are associated with increased HBV replication (11, 12). However, insights into the functional role of B cells in an effective immune response to acute hepatitis B may be better gleaned from examining B cells early (prior to CHB development) and those specific for HBsAg. Peripheral HBsAg-specific B cells are

present at similar proportions in acute, chronic and controlled infection, on HBV treatment, and in vaccinated controls (9, 10, 13–15). However, in people with CHB, HBsAg-specific B cells have decreased proliferative capacity and higher proportion of AtM (mean 30% of HBsAg-specific population), with increased levels of inhibitory markers including PD-1, BTLA, CD22 and FcRL5 (9, 10, 14, 15). While previous studies begin to define phenotypes of HBsAg-specific B cells in CHB, it is not known if these phenotypic changes result from chronic infection or are causally associated with failure to recover during the acute infection.

Understanding the role of B cells in HBV recovery is also imperative in people who are living with HIV-1 due to the high prevalence of HBV/HIV co-infection and the adverse consequences of HIV on CHB (16). Because people with HIV are less likely to develop anti-HBsAg and recover from an acute infection (16, 17) and are more likely to undergo HBV reactivation (18, 19), understanding how HIV affects the HBV-specific B cell response may offer insights to an effective B cell response. Whether HBV-specific B cells are present and affected in HBV/HIV co-infection similarly to the global B cell compartment in HIV mono-infection, such as demonstrating increased proportions of activated subsets (plasmablasts, $CD21^{-}CD27^{+}$ activated memory (AM), AtM) (20) and inflammatory/adhesion molecules (CXCR3, CD11c) (20, 21) on these subsets, remains to be seen.

Because acute HBV infection is frequently asymptomatic, most reports on immune responses in HBV have been confined to assessment of CHB samples isolated years

after acute HBV infection. This raises the question of whether immune signatures observed in these cohorts are a *cause* of failed HBV control or a *consequence* of prolonged HBV exposure. To address this knowledge gap, we assessed a unique longitudinal cohort of participants living with or without HIV who acquired an incident HBV infection. We developed a high-dimensional flow cytometry panel to assess global and HBsAg-specific B cells in these participants (22). We interrogated B cell dynamics at the single-cell and antigen-specific levels to improve our understanding of B cell characteristics and the role of B cell immunity around the acute HBV infection period, including in the context of HBV/HIV co-infection.

Results

Demographic and clinical characteristics

To investigate B cell characteristics associated with HBV outcome, we studied cryopreserved peripheral blood mononuclear cells (PBMCs) from 76 men (44 with HIV-1 and 32 without HIV-1) with incident HBV infection in the Multicenter AIDS Cohort Study (MACS), now the MACS-WIHS Combined Cohort Study (MWCCS) (23, 24). MACS participants were enrolled if they were at risk or living with HIV-1, and were prospectively followed at semi-annual study visits (see Methods). As previously reported for the overall MACS cohort, a subset of men acquired HBV during follow up (25). Of men with incident HBV infection, a higher proportion of men with HIV (MWH) not on active HBV-ART developed CHB (17.5%; 95% CI 8.7-29.9%) than men without HIV (MWoH) (8.2%; 95% CI 3.8-15.0%) (26). For this study, sampling procedures did not randomly select MACS participants and; therefore, do not reflect similar HBV recovery probabilities (see Methods). Rather, given the limited number of participants who progressed to CHB, individuals who met the sampling requirements (see Methods) were *all* selected for assessment in this study, followed by matching on controllers demographics. Of the 44 MWH, 31 controlled the HBV infection (70%) and 13 progressed to CHB (30%). Of the 32 MWoH, 23 controlled the HBV infection (72%) and 9 progressed to CHB (28%). Demographic characteristics stratified by HIV-1 status are in Table 1.

For each participant, up to four time points were analyzed, including (i) pre-HBV infection, (ii) acute HBV infection, (iii) early outcome, and (iv) late outcome, with the latest outcome time points acquired less than two years from the estimated time of incident HBV infection (Figure 1A). At each time point, we utilized a 24-color flow cytometry assay to define main B cell subsets, including global unswitched and class-switched memory and HBsAg-specific B cells (Supplemental Figure 1) (22).

For both MWoH and MWH, the acute time point consisted of three groups based on serologic analysis and eventual outcome of HBV infection (controller 1, controller 2, and CHB). Participants in the controller 1 and CHB groups were HBsAg positive with or without positive HBV DNA while the controller 2 group was already HBsAg negative and anti-HBc positive. Thus, controller 2 group both acquired and controlled their incident HBV infection (as shown by HBsAg clearance) in the six months between pre-infection and acute sampling (Supplemental Figure 2A and Table 2). There was no difference in time between the pre-infection visit and the acute visit in any of the three acute groups (controller 1: median=0.50 years, IQR=0.48-0.56 years; controller 2: median=0.52 years, IQR=0.50-0.62 years; chronic: median=0.51 years, IQR=0.48-0.57 years; p-value = 0.25). Due to lack of significant differences in expression of B cell characteristics despite their differential serological status between controller 1 and controller 2 (Supplemental Figure 2, B-D), we combined the two controller groups for subsequent analysis.

Global B cells are dysregulated in HIV-1 infection.

We first determined HIV-1 dependent B cell perturbations pre-HBV infection in MWH by comparing them to MWoH. Uniform Manifold Approximation and Projection based dimensionality reduction (UMAP) revealed differences in the B cell compartment as demonstrated by different increased density areas between MWoH and MWH (Figure 1B). Median fluorescence intensity (MFI) heatmap overlays for all panel markers are shown (Supplemental Figure 3A). B cell annotation based on manual gating revealed that areas of increased density among MWoH were represented by both unswitched B cell populations ($IgM^+IgD^+CD27^+$ marginal zone (MZ) and $IgM^+IgD^-CD27^+$ IgM-only memory) and class-switched populations ($CD21^+CD27^-$ intermediate memory (IM) and $CD21^+CD27^+$ resting memory (RM)), while the area of increased density among MWH consisted of IgD^+CD27^- naïve (unswitched), AM and AtM (class-switched) subsets. We next confirmed these dynamics by quantifying the frequencies of all traditional B cell subsets pre-HBV infection for total B cells (Figure 1C) and class switched B cells (Figure 1D). MWH showed increased frequencies of transitional B cells ($CD10^+CD27^-$), B1 B cells ($CD24^{-/+}CD38^{-/int}CD27^+CD43^+$), and plasmablasts ($CD24^-CD38^{+/++}$) and decreased levels of total memory B cells (MBC) compared to MWoH (Figure 1C). The class-switched MBC compartment for MWH was skewed towards activation, indicated by fewer IM and RM B cells and increased frequencies of AM and AtM B cells compared to MWoH (Figure 1D). UMAP analysis based on these differential B cell subset abundances resulted in clear separation of MWH and MWoH (Figure 1E). This segregation based on HIV-1 status persisted post-HBV infection in the acute and early/late outcome stages, supporting that HBV infection does not overcome all global B cell differences between MWH and MWoH (Supplemental Figure 3B).

We further investigated the expression of functional markers on MBC subsets in MWH pre-HBV infection (Figure 1F and Supplemental Figure 3C). These markers included chemokine receptors (CXCR3, CXCR5), the co-stimulatory molecule CD86, regulatory molecules (BTLA, CD39), inhibitory Fc receptor CD32, and inhibitory markers associated with chronic infections (PD-1, FcRL5, CD11c, CD22) (22). Consistent with the HIV-1 literature (20, 21), in MWH, AM B cells expressed more CXCR3 and PD-1 than AtM, while both AM and AtM expressed higher levels of FcRL5 and CD11c compared with IM and RM (Figure 1F). These phenotypic expression patterns are also observed on AtM B cells in other chronic infections (21). In contrast, CXCR5, CD86, BTLA, CD39, CD32 and CD22 showed higher expression on IM and/or RM B cells compared with AM and AtM (Figure 1F). We also examined expression patterns on MBC subsets of MWoH prior to HBV infection (Supplemental Figure 3, D and E) and compared to MWH (Figure 1G). The expression of activation/exhaustion markers (e.g. CD86, PD-1, CD11c) on IM and RM B cells in MWH were increased compared to MWoH irrespective of HBV infection stage (Figure 1G). Overall, the pre-HBV infection samples demonstrate a B cell compartment skewed toward activation and/or exhaustion in MWH, consistent with previous reports. Most of the phenotypic B cell differences between men with and without HIV were in the IM and RM subsets and persisted throughout the HBV infection course.

Limited global B cell characteristics correlate with HBV outcome.

Having established baseline differences in global B cells based on HIV-1 infection, we next sought to interrogate global B cell dynamics throughout the course of HBV infection to identify features associated with HBV outcome. UMAP based on the abundance of all manually gated B cell subsets across each time point, irrespective of HIV-1 status, revealed considerable overlap by HBV outcome alone between controllers and CHB (Figure 2A). Thus, overall B cell subset composition was not associated with control of an HBV infection. Given the observed effect of HIV-1 on the B cell compartment, we performed all subsequent analyses comparing HBV outcome by first stratifying on HIV-1 status.

To gain more granular insights into HBV-dependent immune dynamics, we compared all manually defined immune characteristics (frequency and MFI; N=370) at each time point between controllers and CHB, stratified by HIV-1 (See Methods, Table S1). Statistically significant differences were observed most often during the post-acute period when comparing CHB to controllers, and nearly all were in MWH. Of the characteristics identified, the frequency of AtM B cells and CXCR5 expression on transitional B cells were significantly higher and lower, respectively, at outcome time points in those with CHB compared to controllers (Figure 2, B and C). In addition, expression of CD86 on multiple unswitched and memory B cell populations was significantly higher in MWH who developed CHB compared to controllers at both acute and outcome time points (Figure 2D and Supplemental Figure 2, C and D). Our results show that the differential immune signature signified by increased CD86 expression occurs during acute HBV infection between individuals who develop CHB versus control and persists in the post-acute

period. Additional signatures including increased frequency of AtM B cells and decreased expression of CXCR5 on transitional B cells are observed only in the post-acute period.

For each of the characteristics identified above in MWH, we next stratified participants progressing to CHB based on CD4 count and observed that those with low CD4 counts (<350 cells/mL) had significantly higher frequencies of AtM B cells and CD86 expression or lower CXCR5 expression compared to controllers (Figure 2E). CXCR5 expression on transitional B cells was also significantly lower in CD4 low CHB participants when directly compared with CD4 high (>350 cells/mL) CHB participants. Taken together, MWH who progressed to CHB had higher frequencies of AtM B cells and CD86 expression on multiple B cell subsets, and lower CXCR5 expression on transitional B cells at acute and/or outcome time points. These observations were significantly more pronounced with lower CD4 count. In contrast, MWoH had stable proportions of cells and expression of these molecules throughout their HBV infection regardless of HBV outcome.

Unsupervised clustering reveals a unique population of B_{reg} cells upregulated in CHB at outcome in MWH.

Manual gating analysis is limited to biological knowledge and does not take the full dimensionality of the data into account (27). Thus, interesting immune phenotypes may be missed. To capture the phenotypic heterogeneity of B cells, we used unsupervised clustering (FlowSOM) from B cells in all 244 samples (17.5 million cells) to define 40 unique clusters (28). Overlay of the cluster annotation on UMAP of global B cells from all

time points revealed heterogenous B cell phenotypes based on their unique locations on the UMAP (Supplemental Figure 4A). The average FlowSOM cluster frequency ranged from <0.1% to >30% and a heatmap of all markers for each cluster is shown (Supplemental Figure 4B).

Next, we assessed if FlowSOM cluster abundance differed based on HBV outcome at any time point. We again delineated individuals based on HIV-1 status due to profound HIV-dependent B cell perturbations. Multiple clusters significantly differed between HBV controllers and CHB groups in either MWH or MWoH (N=12) (Figure 3A). Marker expression for these clusters is shown (Supplemental Figure 4C) and the heatmap revealed further clustering into three groups (Supplemental Figure 4D), driven by CD11c, CD27 and CD10, respectively, as shown by principal component analysis (PCA) (Supplemental Figure 4E).

While multiple clusters were significantly altered at a given time point, only two clusters, #14 and #31, differed at multiple time points and were selected to further explore (See Methods). Clusters #14 and #31 were significantly increased in CHB compared to controllers at multiple time points for MWoH and MWH, respectively (Figure 3A, red circles). Cluster #14 differed at non-consecutive acute and late outcome in MWoH and was characterized by IgM^{+}, IgD^{+}, $CD27^{lo}$, $CD21^{lo}$, $CXCR5^{+}$, $CD11c^{+}$, and $FcRL5^{+}$, likely representing activated naïve B cells (Supplemental Figure 4C) (29). In contrast, cluster #31 differed consecutively at both early and late outcome time points in MWH, supporting a robust association with CHB (Figure 3B). Cluster #31 consisted of transitional-like B

cells ($CD10^{+}IgM^{+}IgD^{+}CD5^{hi}CD24^{hi}CD38^{hi}CD21^{-}CD32^{-}CD27^{-}$) with heterogenous expression of functional markers (Figure 3, C and D). Amongst MWH, cluster #31 abundance was also significantly higher in those with low CD4 count progressing to CHB compared to either those with high CD4 count progressing to CHB or those in the controller group (Figure 3E). This combination of lineage markers in association with progression to CHB suggests that cluster #31 represents regulatory B cells (B_{regs}). Although production of IL-10 is the gold standard to identify B_{regs}, transitional B cells expressing CD24, CD38, and CD5, as the cluster #31 cells do, have been previously shown to secrete IL-10 and have been described as B_{reg} populations (30). Altogether, FlowSOM cluster analysis reveals a unique B_{reg} population in MWH with significantly higher abundance in CHB versus controllers and in MWH with low versus high CD4 counts.

HBsAg-specific B cells expand in MWoH who control HBV and comprise distinct clusters.

We next interrogated HBsAg-specific B cell dynamics and phenotypes based on HBV outcome given their importance in prevention and control of HBV. Representative manual gating of HBsAg-specific B cells using a dual probe strategy is shown (Figure 4A). HBsAg-specific B cells ranged from undetectable to 1.13% total B cells (median 0.013%). Longitudinal sampling enabled us to uniquely assess the HBsAg-specific B cell dynamics within each participant by calculating the fold-change of frequencies over baseline (pre-HBV infection) (Figure 4B). We observed significant expansion in HBsAg-specific B cells

291 in MWoH only in participants who controlled their HBV infection. No expansion was
292 observed in MWoH who progressed to CHB, or in MWH, regardless of HBV outcome.
293
294 We also examined HBsAg-specific B cell frequencies cross-sectionally, similar to
295 previously published analyses (9, 10, 13, 14). Here, we observed that MWoH who
296 controlled their HBV infection showed significantly higher HBsAg-specific B cell
297 frequencies at outcome time points compared to pre- and acute infection while chronic
298 HBV infection did not show an increased abundance of HBsAg-specific B cells
299 (Supplemental Figure 5A). In contrast, MWH who ultimately controlled HBV infection had
300 significantly higher HBsAg-specific B cell frequencies compared to CHB only during acute
301 infection, not at outcome time points. When comparing MWoH to MWH, we observed
302 significantly increased HBsAg-specific B cell frequencies in MWoH during the acute stage
303 in those who progressed to CHB and during early outcome in the HBV controllers
304 (Supplemental Figure 5B). HBsAg-specific B cell frequencies were not altered in MWH
305 on treatment (N=8, Supplemental Figure 5C). Stratifying the three acute groups
306 (controller 1, controller 2 and chronic) revealed a significantly higher HBsAg-specific B
307 cell frequency in controller 2 compared to participants with subsequent chronic HBV
308 infection within MWH (Supplemental Figure 5D).
309
310 We then stratified the previously generated UMAP of total B cells based on time point,
311 HIV-1 status and HBV outcome and overlaid HBsAg-specific B cells (Figure 4C). We
312 observed the HBsAg-specific B cell expansion in MWoH occurred in specific UMAP
313 locations, suggesting unique B cell subsets. HBsAg-specific B cells were detected at

various frequencies in 39 of the 40 FlowSOM clusters (Supplemental Figure 5E). UMAP and FlowSOM analysis revealed that expanded HBsAg-specific B cells in MWoH controllers consist of multiple phenotypically distinct B cell subsets, primarily RM and IM MBCs (Figure 4D; Supplemental Figure 4B for FlowSOM cluster marker expression patterns).

Overall, unlike the global B cell analysis demonstrating HBV outcome-related differences primarily in MWH with CHB, HBsAg-specific B cells expanded only in MWoH controllers. These cells expanded within distinctive areas of the UMAP projection, indicating potentially protective phenotypes that merited further interrogation.

Expanded HBsAg-specific B cells are phenotypically heterogeneous.

Next, we assessed if the frequency of HBsAg-specific B cells in any of the 39 FlowSOM clusters differed between time points to identify specific phenotypes associated with expansion upon HBV infection. Volcano plots stratified by HBV outcome and HIV-1 infection status revealed significant expansion of HBsAg-specific B cells in 12 FlowSOM clusters only in HBV controllers (Figure 5A). No differences occurred in CHB (Supplemental Figure 5F). All but two of the clusters identified were from MWoH and significantly differed between pre-infection/acute vs outcome time points. This is consistent with our data showing expansion of total HBsAg-specific B cells in MWoH at the HBV infection outcome time points versus pre-infection. Grouping the 10 clusters that

significantly differed by at least two time points (See Methods) based on HIV-1 status (MWoH, clusters #4, #9, #16, #23, #24, #27, #28, #33; MWH, clusters #10 and #15) demonstrated significantly increased frequencies only during outcome time points (Figure 5B). The total number of B cells per sample were consistent across time points, regardless of HIV-1 status and HBV outcome, indicating that HBsAg-specific B cell frequencies did not merely reflect sampling differences (Supplemental Figure 5G).

We next sought to investigate the phenotypes of these clusters to gain in-depth insights into the phenotypic landscape of antigen-specific B cell expansion in HBV infection (Figure 5, C and D). Expression levels of all markers assessed in the panel were plotted by histogram and compared with total B cells (cluster #0, grey histogram). For MWoH, significantly expanded HBsAg-specific B cells consisted of clusters which resembled $IgM^+IgD^+CD21^+CD27^-$ naïve B cells (cluster #4), $IgM^-IgD^-CD21^{+/int}CD27^+$ IM and RM B cells (clusters #16, #23, #24, #27 and #28) and $IgM^-IgD^-CD21^-CD27^{lo}$ AtM B cells (cluster #9) (Figure 5C). Cluster #33 appeared to be a mixed cluster consisting of negative to intermediate expression of all lineage markers assessed. For clusters upregulated in MWH (clusters #10 and #15), both demonstrated lineage marker expression of $IgM^+IgD^{int}CD21^-CD27^{int/+}$ consistent with activated naïve and/or MZ B cells.

Further analysis of phenotypic markers demonstrated heterogeneous phenotypes between the IM and RM B cell clusters from MWoH (Figure 5D). For example, clusters #23 and #24 showed higher expression of CD86, CD11c and FcRL5, markers of both activation and exhaustion, compared to clusters #16, #27 and #28. In addition, clusters

#16 and #27 are characterized by increased expression of lymph node trafficking marker CXCR5 compared with #23 and #24. In contrast, clusters #10 and #15, which resemble naïve and/or MZ B cell subsets in MWH, demonstrated expression of multiple inhibitory and/or putative inhibitory markers including CD11c, FcRL5, CD22, and CD32 (Figure 5D). Interestingly, no selected clusters expressed PD-1 and unlike the global B cell analysis, there was limited CD86 expression in these clusters.

Overall, in MWoH, HBsAg-specific B cell expansion was observed upon HBV outcome, and these cells demonstrate heterogeneous phenotypes associated mainly with resting and intermediate MBCs. For the two unswitched B cell clusters that minimally expanded in MWH, their phenotypic marker expression is consistent with dysfunctional naïve-like HBsAg-specific B cell subsets. As these clusters were identified in controllers, the phenotypes may represent a sub-optimal B cell compensatory mechanism in people with HIV-1 to manage subsequent infections.

Discussion

Here, we provide a comprehensive longitudinal assessment of global and HBsAg-specific B cell dynamics in peripheral blood sampled prior to, during, and after established outcome for acute HBV infection. Our study evaluates B cell function in the largest longitudinal collection of participants with incident HBV. Importantly, over half of the participants included were living with HIV-1 at the time of HBV infection, allowing us to additionally interrogate B cell characteristics in the context of HBV/HIV co-infection. Prior studies have described widespread HIV-associated B cell perturbations (20, 31–33), which we confirmed in our cohort and followed through an acute HBV infection, demonstrating that HIV-1 negatively affects HBV infection responses, both at the global and the antigen-specific B cell level. Interestingly, no global B cell characteristics significantly differed in MWoH based on HBV outcome. This suggests that in mono-infection, global B cells remain minimally affected around the acute infection period, consistent with observations that people with CHB can respond normally to vaccination or subsequent infections (34, 35).

Multiple global B cell characteristics significantly differed based on HBV outcome between CHB and controllers in MWH. We identified decreased expression of CXCR5 on transitional B cells, increased frequencies of B_{regs}, elevated CD86 expression on multiple unswitched and MBC subsets, and increased AtM B cell frequencies in individuals with CHB. These differences were not present prior to HBV infection, developing in MWH only after incident HBV, suggesting that baseline B cell differences did not pre-dispose to CHB

development and that precedent HIV-1 infection may drive adverse B cell changes over the course of CHB.

The lower expression of CXCR5 on transitional B cells observed in our study may impair replenishment of B cells. CXCR5 recruits mature B cells to lymph nodes to promote entrance into germinal centers for mounting productive antiviral responses (36). $CD10^+$ transitional B cells are elevated in chronic viral infections, potentially as a compensatory reaction to the loss of naïve B cells and to increased B cell activation (37). However, the role of CXCR5 on transitional B cells and its implications in HBV infection warrants further investigation.

In addition, we observed higher frequencies of B cells with phenotypes consistent with B_{regs} in CHB compared to controllers in MWH. While FlowSOM cluster #31 shows similarities with transitional B cells based on CD10, CD24, and CD38, their unique phenotypic characteristics suggest regulatory functions, as described previously. For instance, CD5 expression has been associated with reduced T cell proliferation and increased expression of IL-10 upon *in vitro* stimulation (38, 39). In addition, the reduced expression CD21 and CD32 on cluster #31 matches the phenotypic characteristics of $CD24^+CD38^+$ transitional B cells with regulatory functions (40). Thus, based on these observations, we concluded that cluster #31 consists of B_{regs}. B_{regs} have been reported in CHB mono-infection and contribute to a dampened $CD8^+$ T cell response that may allow for chronic infection to persist (11, 12). The $CD8^+$ T cell response is crucial for control of HBV and impaired $CD8^+$ T cell activation may hamper the development of protective

cytotoxic T cell responses (41). Thus, the combination of HIV-1 infection induced T cell perturbations (42) and the observed increase in B_{regs} may further hinder control of HBV infection.

The co-stimulatory receptor CD86 is upregulated upon B cell activation and is a crucial co-stimulatory molecule for optimal T cell activation (43, 44). Viral infections lead to the expansion of $CD21^{-}$T-bet^{+} B cells, which express high levels of CD86 and have similar phenotypes to AM and AtM B cells (45). T-bet^{+} B cells persist in chronic viral infections such as HIV-1 and CHB and are thought to be both a source of antiviral immunoglobulin (9, 45) but are also associated with B cell exhaustion in the context of chronic antigen exposure (21, 46). In CHB, T-bet expression is increased in AtM B cells with higher frequencies of inflammatory homing markers CD11c and CXCR3 expression (9). While we did not measure T-bet, the combination of increased abundance of AtM B cells and elevated expression of CD86 on various B cell subsets within MWH with CHB may reflect the expansion of an activated, antiviral B cell population driven toward exhaustion by aberrant trafficking to inflamed sites such as the liver in CHB.

AtM B cells are present in circulation of healthy individuals (3-5% total B cells) and may represent a short-lived lineage that can expand upon infection or vaccination (47, 48). However, during persistent antigen exposure, they can expand to over 50% and appear terminally differentiated and functionally inferior, with upregulation of exhausted-like inhibitory markers and less somatic hypermutation than their RM counterparts (21, 49, 50). Consistent with a negative functional consequence, we observed significantly

443 increased AtM B cell frequencies in MWH with CHB compared to controllers. Of note,
444 AtM B cell expansion has been reported in multiple long-term CHB mono-infection cohorts
445 (9, 10, 51), while we see expansion only in HBV/HIV co-infection. Previous studies were
446 conducted with participants many years after developing CHB while our samples were
447 collected relatively shortly after acute infection (within 2 years, mean time 1.66 years).
448 The discrepancy between our data and previous reports may reflect prolonged antigenic
449 exposure in HBV mono-infection. Clinically, infection with HIV-1 prior to HBV exposure
450 increases an individual's risk of developing CHB six-fold (16, 17) and within the MACS
451 cohort, MWH not on active HBV-ART had a higher proportion of those with incident HBV
452 develop CHB (17.5%) compared to MWoH (8.2%) (26). In addition, HIV-1 co-infection
453 accelerates CHB associated end-stage liver disease, cirrhosis and HCC (52). Thus, AtM
454 expansion in HIV-1 co-infection, as well as the other phenotypes we observed only in
455 MWH, may reflect acceleration of a process that occurs over a longer period in CHB
456 without HIV-1 co-infection. This hypothesis is supported by our results in MWH with low
457 CD4 counts showing significantly more pronounced immune perturbations in CHB.
458
459 A key feature of our B cell panel is the inclusion of HBsAg probes to identify ex vivo
460 HBsAg-specific B cells longitudinally. The analysis of HBsAg-specific B cells also
461 revealed a negative impact of HIV-1 on HBV, with limited HBsAg-specific B cell expansion
462 in MWH. This failure of HBsAg-specific B cell expansion may restrict the anti-HBsAg
463 response in co-infection. In support of this finding, clinical studies demonstrate that adults
464 with HIV-1 mount a limited anti-HBsAg response to standard recombinant HBV
465 vaccination compared with healthy individuals (53). In addition, HIV-1 infection leads to

466 higher rates of reactivation of controlled HBV infection (18, 19), which may be partially
467 attributable to the fact that people with HIV-1 are unable to sufficiently expand their
468 HBsAg-specific B cell pool to maintain long-term HBV control. Although MWH failed to
469 expand HBsAg-specific B cells, our cohort consisted of 31 participants who controlled
470 their incident HBV infection. This suggests that in these individuals, additional immune
471 populations such as effector T cell functions may be involved in HBV control. New
472 evidence suggests TCF-1^{+}CD127^{+}PD-1^{+} precursor to exhaustion (Tpex) HBV-specific
473 CD8^{+} T cells may contribute to control in the context of HIV/HBV co-infection (54).
474
475 In contrast, we found that in MWoH, HBsAg-specific B cells did expand, with significantly
476 increased frequencies in controllers within 6 months to 2 years after acute infection. We
477 did not see this B cell expansion during acute infection, when productive immune
478 responses against HBV are first presumably being mounted, suggesting an overall delay
479 in HBsAg-specific B cell induction and highlighting the potential importance of HBV-
480 specific T cell responses during acute HBV control. A technical limitation to the HBsAg
481 probe approach is that in samples with endogenous anti-HBsAg bound to HBsAg (acute
482 and CHB samples), our ability to fully quantify HBsAg-specific B cells as soon as antibody
483 is produced was likely negatively affected. However, if the detection of HBsAg-specific B
484 cell expansion in MWoH controllers were solely due to loss of HBsAg, we would also
485 expect to see similar expansion in MWH controllers.
486
487 Unlike previous reports that characterize HBsAg-specific B cells in CHB (9, 10, 13–15),
488 we focused our phenotypic analysis on intra-participant expanded HBsAg-specific B cells

to interrogate potential signatures of productive antigen-specific responses in HBV. Expanded HBsAg-specific B cells were predominantly in MWoH controllers at outcome and consisted mainly of class-switched (non-IgM expressing) IM and RM subsets. IM and RM antigen-specific B cells have been shown to expand upon control of SARS-CoV-2 infection (55) and are important for recall response to reinfection (56). In addition, HBsAg-specific B cells in CHB with treatment-associated HBsAg loss or seroconversion (functional cure) exhibit higher proportions of $CD21^{+}CD27^{+}$ RM B cells, suggesting this population is important for maintaining HBV control (14, 15). High-dimensional single-cell approaches like the method we employed enables a more granular assessment of B cell subsets. For example, despite their shared memory B cell annotation, expanded IM and RM subsets revealed heterogenous phenotypes, suggesting the definition of memory B cells may go beyond conventional CD21 and CD27 expression patterns. We observed a group of clusters with either less (#16 and #27; $CXCR5^{+}$, $CD86^{-}$, $PD\text{-}1^{-}$, $FcRL5^{-}$, $CD11c^{-}$) or more (#23 and #24; $CXCR3^{+}$, $CD86^{+}$, $BTLA^{+}$, $FcRL5^{+}$, $CD11c^{+}$) activated signatures. Interestingly, these activated clusters appear phenotypically similar to AtM B cells based on the increased expression of FcRL5 and CD11c, and downregulation of CXCR5. Therefore, our data suggests an activation and differentiation continuum within the HBsAg-specific B cell compartment which may be required for productive and sustained HBV control in MWoH.

This study had multiple limitations due to the cohort studied. First, the findings described here were generated from an all-male cohort and may differ in women as immune responses are known to differ by sex. Second, since the participants came to semi-annual

visits, sampling at the peak of their acute infection was not always feasible and the time between the acute infection and the sampling is not uniform. Third, all samples were obtained from peripheral blood draws, limiting our assessment to circulating B cells rather than the liver, the site of HBV infection. However, previous studies have identified phenotypes of circulating B cells to be present but enriched in the liver in HBV infection (9). Finally, the limited cell numbers available for each participant precluded subsequent in vitro testing to further interrogate functional consequences of the phenotypic signatures described by the ex vivo analysis.

Altogether, these results identify HIV-associated B cell alterations that elucidate potential mechanisms for previously identified negative effects of HIV-1 on HBV control. Multiple B cell subsets associated with dysregulation in antiviral responses were significantly upregulated in CHB in MWH alongside failure to expand an antigen-specific B cell response. In contrast, global B cells in HBV mono-infection showed no differences by HBV outcome and HBsAg-specific B cells expand during HBV control. These antigen-specific B cells consist mainly of IM and RM subsets with heterogenous activation phenotypes. Our observations support a role for B cells in HBV control of acute infection and warrant further functional examination to fully characterize HBsAg-specific B cells in acute and ongoing HBV control.

Methods

Sex as a Biological Variable

All participants in this study were XY male and identified as men. This choice was guided by the access and availability of samples in the all-male MACS cohort, however, men demonstrate a higher incidence of CHB and HCC with poorer prognosis compared to women (57, 58).

Study Participants

Male participants followed semi-annually in the Multicenter AIDS Cohort Study (MACS) (25) (now part of the MACS-WIHS Combined Cohort Study) (23) who had, or were at risk for, HIV-1 infection and had an incident HBV infection during follow-up, were considered for inclusion. In the MACS, biological specimens including plasma and PBMCs are collected and stored at each study visit. Incident HBV was identified through retrospective serologic analysis, as previously described (24). Briefly, incident HBV infection was defined in participants who were negative for HBsAg, anti-HBc, and anti-HBs who seroconverted to anti-HBc positivity during follow-up. The estimated date of incident HBV infection was defined as the midpoint between the last negative and first positive anti-HBc or -HBsAg test result, whichever was positive first (24). The outcome of the incident HBV infection, HBV recovery (controller) or CHB, was defined based on serologic testing, as previously described (26). Briefly, CHB was defined by at least two positive HBsAg tests $\geq$ 6 months apart and controller was defined as at least one visit negative for HBsAg and positive for anti-HBc at a visit within 18 months after the incident infection.

555 Men with incident HBV were included in this study if PBMCs were available prior to
556 incident HBV infection (pre-infection, -0.5 to 0 years from estimated incident infection), at
557 the first visit positive for anti-HBc or HBsAg (acute infection, 0 to 0.5 years), and/or 0.5-2
558 years after the estimated date of incident infection (early outcome, 0.5 to 1.5 years; late
559 outcome, 1.5 to 2 years) (Figure 1A; Table 1 and Table 2). We matched all men with
560 known CHB who had PBMCs available at these time points to men with known HBV
561 recovery (controllers) at a minimum 1:1 (CHB to controller, 4 groups), but where possible,
562 we matched 1:2 (10 groups), 1:3 (8 groups) or 1:5 (1 group) based on age, HIV-1 status,
563 CD4 T cell count (for MWH), and time samples were stored in the repository. We included
564 76 men of whom 54 were HBV controllers and 22 had CHB. Of the 76 men included, 44
565 were living with HIV-1 and 32 were not for all time points assessed. For most participants
566 included in the study, seropositivity for HBsAg, anti-HBc, anti-HBs and HBV DNA levels
567 are available, as well as antiretroviral therapy for those participants receiving HIV-1
568 treatment (N = 8) (Table 1 and 2). HBV DNA was measured only at the acute HBV time
569 point. All participants on treatment remained so throughout the entire time course
570 assessed here. HIV viral load and CD4 counts were also measured at all time points and
571 did not significantly differ by HBV infection status. Not all participants had samples
572 available for all 4 time points (21 participants lacked one of two outcome samples, 9
573 participants lacked samples from both outcome time points, and 4 participants did not
574 have a pre-infection sample available). A total of 262 samples were included for
575 processing and staining.
576
577 ***Sample Processing and Flow Cytometry Staining***

PBMCs were cryopreserved in FBS + 10% DMSO and stored in liquid nitrogen until use in this study. PBMC processing and flow staining were performed using the pipeline previously described (59). Briefly, cryopreserved PBMCs were thawed in 37°C pre-warmed RPMI + 10% FBS (R10) using the Thawsome adaptor (Medax International, Inc.) (60). Cells were washed once in 5mL R10, then centrifuged at 860 x *g* for 3 min and transferred to V-bottom 96-well plates for immediate B cell panel staining.

All flow cytometry antibodies and staining reagents used for this study are in Supplemental Table 2 and are further described in detail in Cascino et al. 2020 (22). The panel was designed to define comprehensive B cell subsets (Supplemental Figure 1). For the antigen-specific B cell probe, we obtained recombinant small hepatitis B surface antigen (HBsAg) genotype C, manually conjugated to one of two fluorochromes, Dylight 550 or Dylight 650, from Gilead (22, 61).

Antibody staining cocktail containing all but the antigen-specific B cell probes were prepared in advance and stored at 4°C before staining the next day. Immediately prior to B cell staining, 0.2ug/50uL reaction of each antigen-specific B cell probe was added and centrifuged at 15,000 x *g* for 5 min to remove dye aggregates. PBMCs were washed twice in 200uL phosphate buffered saline (PBS) prior to staining with Fixable Live/Dead Aqua (Thermo Fisher Scientific) for 20min at 4°C. Samples were then washed twice in 200uL PBS and stained with 50uL staining cocktail for 30min at 4°C in the dark. After incubation, samples were washed twice with 200uL staining buffer (PBS + 0.5% bovine serum albumin (BSA)) and subsequently fixed for 20min with 2% paraformaldehyde (PFA) at

4°C. After fixation, cells were washed once with staining buffer, resuspended in 250uL 0.5% PFA, and stored at 4°C in the dark until acquisition the next day on a BD FACSymphony A5 cytometer using FACS DIVA software (version 9.3.1). The flow cytometers were standardized to ensure consistent and reproducible performance according to Perfetto et al. (62, 63).

The total 262 samples were processed in four batches. Matched participants were randomized to one of the four batches and all samples for those participants were included in the same batch to mitigate potential issues with batch effects. PBMCs from the same blood draw from an unexposed healthy individual were measured in all experiments as a technical control to assess reproducibility and for data normalization (59).

Flow cytometry data pre-processing

Flow cytometry data pre-processing is critical to remove low quality data and prevent artificial data output. We used the R-implemented (R version 4.0.0) algorithm FlowAI (version 1.18.5) (59) for automated removal of irregular events and outliers, which can arise from fluctuations in flow cytometer performance. In 222 out of 262 samples, FlowAI detected minor irregular events (<10%), which were removed automatically. For the remaining 40 samples with more than 10% irregular events, we manually inspected the raw data to prevent excessive data loss (64). 20 of these samples required manual removal of irregular events.

Subsequently, correction for spectral overlap (compensation) was performed in FlowJo 10.1.7 (BD Biosciences) using single-stained beads. Persisting compensation inaccuracies were corrected manually.

We performed preliminary gating of viable $CD19^{+}CD20^{+}$ B cells with FlowJo 10.9 and exported a new set of fcs files for subsequent analysis of immune cell characteristics. The precision of flow cytometric analysis depends on Poisson statistics and thus requires sufficient cell counts. To this end, four samples were excluded from analysis due to limited B cell counts (<5,000 B cells). 14 additional samples were removed from analysis to avoid duplication of samples in each of the four longitudinal groups (pre-infection, acute, early outcome, late outcome) from a single participant. A total of 244 samples were included for analysis moving forward.

Manual flow cytometry analysis

Manual gating was performed using FlowJo 10.9. Markers were divided in two groups based on their purpose to either define immune cell subsets (lineage markers) or functional markers/characteristics (Supplementary Table S2). Manual gating strategy can be found in Supplemental Figure 1 and Cascino et al. (22).

Three different parameters were extracted for subsequent analysis: frequency of immune cell populations, frequency of cells expressing functional markers and geometric mean fluorescence signal (MFI).

Unsupervised data analysis

Based on the technical control samples we observed batch-to-batch variation between the four experiments. Our manual gating analysis accommodates for batch variation by applying cut-off gates on a per-experiment basis. However, non-biological inter-assay data variation will negatively impact the accuracy of unsupervised data analysis (27, 59). Therefore, we normalized the flow cytometry raw data using CytoNorm (65). To this end, we concatenated all files per experiment to train the CytoNorm model, which was applied to the aggregated files as described (66). The normalized flow cytometry data was used for subsequent unsupervised data analysis with concatenated fcs files. Samples were identifiable by sample-specific keywords. R (version 4.2.1) programming language with RStudio (2023.06.0 Build 421) interface was used for unsupervised data analysis. Raw data (fcs files) containing concatenated B cells were imported using the flowCore (version 2.10.0) package. Data were transformed using the estimateLogicle function from the flowCore package.

For dimensionality reduction algorithm UMAP (version 0.2.10.0) (67) and FlowSOM clustering analysis we combined all HBsAg-specific B cells (N = 5,321) with 1000 randomly selected B cells per sample (total 244k B cells from 244 samples; 109k B cells from MWH, 135k B cells from MWoH) to generate UMAP projection and define cluster abundances for total and antigen-specific B cells from all time points. HBsAg-specific B cells were defined based on co-staining of the two B cell probes. A cut-off of 1.8 and 1.9 was used for logicle-transformed signal from Dylight650 and Dylight550 conjugated probes, respectively (Figure 4, C and D). For UMAP, default settings were used and all

markers except the HBsAg-specific B cell probes and viability/dump markers were used. To visualize expression levels on the UMAP, logicle-transformed fluorescence intensity values were normalized based on 1% and 99% percentile. Figure 1B is based only on pre-infection total B cell composition between MWoH and MWH. Here, UMAP was visualized based on 800 and 1000 randomly selected B cells per MWH (N = 40) and MWoH (N = 32) to obtain equal numbers of B cells between HIV-1 infection status (n = 32,000 cells per group). In Figure 1E, 2A and Supplemental Figure 3B, UMAP algorithm based on 16 non-normalized manually gated B cell subset frequencies were used to define unique immune compositions between MWH and MWoH (Figure 1E and Supplemental Figure 3B) and controller and CHB (Figure 2A) where each dot represents one sample.

For visualization of HBsAg-specific B cells in either UMAP or biaxial raw data, one participant was removed due to large expansion of HBsAg-specific B cells which affects the visualization of rare HBsAg-specific B cells from other samples. The HBsAg-specific B cells from this participant were included for statistical analysis.

Clustering of B cells from all 244 samples (N = 17,432,605) was performed using FlowSOM (version 2.4.0). FlowSOM parameters included a cluster grid of 20 x 20 and in a subsequent step 40 metaclusters were defined. Fluorescence signals from all markers (N =21) except for viability dye and the two antigen-specific B cell probes were used to compute FlowSOM clustering. Manual gating designation was extracted from FlowJo workspace using the GetFlowJoLabels function from the FlowSOM package.

The heatmap showing median fluorescence intensity for each marker per cluster (Supplemental Figure 4B) was created with the pheatmap package (version 1.0.12) and input data was normalized using 1% and 99% percentile normalization. The ggplot2 (version 3.4.4) package was used for data visualization. Overlay histograms depicting expression of markers per cluster was performed using the ggridges package (version 0.5.5). To this end, 10,000 B cells were randomly selected across all samples to visualize expression on total B cells.

Statistical analysis

Statistical comparisons were performed in GraphPad Prism 10 or R. Comparison between conditions were performed using non-parametric tests with or without correction for multiple testing as indicated in figure legends. A p-value less than 0.05 was considered significant except for analysis in Figure 5B where we visualized FlowSOM clusters, which had at least one significant difference with a p-value < 0.01 to highlight the differences that remained statistically significant using a more conservative type 1 error threshold.

For the exploratory analyses in Figures 1G, 2B-D, 3 A and B, and 5A, we tested the difference of 40-370 unique immune characteristics between CHB and HBV controllers in four time points (Supplemental Table 1). Thus, our sample size is not sufficiently large for multiple testing correction with such comprehensive lists of distinct immune characteristics. Therefore, we focused our analysis on specific immune characteristics as follows. For Figure 1G, we show all phenotypic immune characteristics with a p-value < 0.05 by Wilcoxon ranked-sign test (BTLA, FcRL5 and CD22 demonstrated no significant

differences). For the remaining figures, immune characteristics selected to highlight in the figures were only those characteristics that significantly differed in consecutive time points (Figures 2, B and C; Figure 3, A and B; Figure 5A) and/or between multiple immune characteristics (manually gated frequency and MFI; Figure 2D). Finally, for the analysis in Supplemental Figure 2B, we first assessed the differences between the two controller groups and CHB at the acute time point using Kruskal-Wallis rank test. Those significant characteristics were then compared between the acute groups by Wilcoxon signed-rank test in Supplemental Figure 2C which primarily revealed CD86 expression to be significantly different. Thus, we focused our analysis in Supplemental Figure 2D on CD86 expression in various B cell subsets to visualize significance of CD86 expression between all three acute groups (controller 1, controller 2 and chronic) as determined by Wilcoxon signed-rank test.

In Figure 5, frequency of HBsAg-specific B cells within the 40 B cell clusters was calculated. Wilcoxon signed-rank test without correction for multiple testing was used to identify significant differences in HBsAg-specific B cell abundance within FlowSOM clusters between time points and per HIV infection status and HBV outcome (Figure 5A and Supplemental Figure 5F). For multiple clusters (#2, #17, #19, #22, #32, #34, #35, #36, #38 and #39), differences could not be assessed due to insufficient HBsAg-specific B cells between the two groups in at least one sampling time point.

12 FlowSOM clusters were identified in Figure 5A with at least one significant difference ($p < 0.01$). Of these clusters, we selected to further analyze 10 clusters of interest in

Figure 5B under the following criteria: the two clusters significantly upregulated for MWH (clusters #10 and #15) and only the 8 clusters significantly upregulated at two or more time point comparisons (clusters #4, #9, #16, #23, #24, #27, #28 and #33). In Figure 5B we then performed Wilcoxon signed-rank test with Bonferroni correction for multiple testing to determine statistically significant differences in longitudinal HBsAg-specific B cell abundances in our clusters of interest. Of note, the remaining clusters from Figure 5A (#13 and #18) did not show any significant differences between time points after Bonferroni correcting for multiple testing.

Finally, to incorporate all available longitudinal data in comparisons of expression levels across multiple timepoints, we fit generalized estimating equation (GEE) models using SAS proc GENMOD which accounts for the resulting correlated data structure (Figure 2E and Figure 3E). In these GEE analyses, we modeled the natural-log transformed immune expression data as the dependent variable and chose to account for the correlated data using an autoregression correlation structure after examining model fit results.

Study approval

All participants provided written informed consent for this study. This study was approved by the Institutional Review Board at Johns Hopkins University.

Data Availability

Data values for all graphs are provided in the Supporting Data Values file.

Author Contributions

KC and TL (co–first authors) contributed equally to designing and conducting experiments, acquiring and analyzing data, and preparing figures for publication. KC had primary responsibility for planning, scheduling experiments, and drafting the manuscript and is therefore assigned as lead co–first author. ES contributed to data interpretation. KS contributed to flow cytometry panel design. SW, MW and RM contributed to sample acquisition and manuscript review. MR provided facilities and contributed to manuscript review. JB contributed to data interpretation and manuscript review. AC, CT conceived and supervised the study, contributed to data analysis, interpretation and manuscript review.

Funding Support

This work is the result of NIH funding, in whole or in part, and is subject to the NIH Public Access Policy. Through acceptance of this federal funding, the NIH has been given a right to make the work publicly available in PubMed Central. Support for this work was provided in part by the Vaccine Research Center, an intramural Division of National Institute of Allergy and Infectious Diseases, National Institutes of Health by a grant from the Foundation for the National Institutes of Health through the Collaboration for AIDS Vaccine Development of the Bill & Melinda Gates Foundation grant OPP1147555 to TL and MR, and in part by the National Institute of Allergy and Infectious Diseases grant R01AI116269 to CT and AC. All funding sources had no role in study design; in the collection, analysis, and interpretation of data; in the writing of the report; and in the decision to submit the paper for publication.

Acknowledgements

Data in this manuscript were collected by the Multicenter AIDS Cohort Study (MACS), now the MACS/WIHS Combined Cohort Study (MWCCS). We would like to thank the participants in the MWCCS and dedicated staff at the MWCCS sites. We also thank the Vaccine Research Center flow core facility for instrumentation characterization and maintenance. Additionally, we thank Simon Fletcher and Nikolai Novikov of Gilead Sciences for providing conjugated HBsAg.

The contents of this publication are solely the responsibility of the authors and do not represent the official views of the National Institutes of Health (NIH). MWCCS (Principal Investigators): Atlanta CRS (Cecile Lahiri, Anandi Sheth, and Gina Wingood), U01-HL146241; Baltimore CRS (Todd Brown and Joseph Margolick), U01-HL146201; Bronx CRS (Kathryn Anastos, David Hanna, and Anjali Sharma), U01-HL146204; Brooklyn CRS (Deborah Gustafson and Tracey Wilson), U01-HL146202; Data Analysis and Coordination Center (Gypsyamber D'Souza, Stephen Gange and Elizabeth Topper), U01-HL146193; Chicago-Cook County CRS (Mardge Cohen, Audrey French, and Ryan Ross), U01-HL146245; Chicago-Northwestern CRS (Steven Wolinsky, Frank Palella, and Valentina Stosor), U01-HL146240; Northern California CRS (Bradley Aouizerat, Jennifer Price, and Phyllis Tien), U01-HL146242; Los Angeles CRS (Roger Detels and Matthew Mimiaga), U01-HL146333; Metropolitan Washington CRS (Seble Kassaye and Daniel Merenstein), U01-HL146205; Miami CRS (Maria Alcaide, Claudia Martinez, and Deborah Jones), U01-HL146203; Pittsburgh CRS (Jeremy Martinson and Charles Rinaldo), U01-

HL146208; UAB-MS CRS (Mirjam-Colette Kempf, James B. Brock, Emily Levitan, and Deborah Konkle-Parker), U01-HL146192; UNC CRS (M. Bradley Drummond and Michelle Floris-Moore), U01-HL146194. The MWCCS is funded primarily by the National Heart, Lung, and Blood Institute (NHLBI), with additional co-funding from the *Eunice Kennedy Shriver* National Institute of Child Health & Human Development (NICHD), National Institute on Aging (NIA), National Institute of Dental & Craniofacial Research (NIDCR), National Institute of Allergy and Infectious Diseases (NIAID), National Institute of Neurological Disorders and Stroke (NINDS), National Institute of Mental Health (NIMH), National Institute on Drug Abuse (NIDA), National Institute of Nursing Research (NINR), National Cancer Institute (NCI), National Institute on Alcohol Abuse and Alcoholism (NIAAA), National Institute on Deafness and Other Communication Disorders (NIDCD), National Institute of Diabetes and Digestive and Kidney Diseases (NIDDK), National Institute on Minority Health and Health Disparities (NIMHD), and in coordination and alignment with the research priorities of the National Institutes of Health, Office of AIDS Research (OAR). MWCCS data collection is also supported by UL1-TR000004 (UCSF CTSA), UL1-TR003098 (JHU ICTR), UL1-TR001881 (UCLA CTSI), P30-AI-050409 (Atlanta CFAR), P30-AI-073961 (Miami CFAR), P30-AI-050410 (UNC CFAR), P30-AI-027767 (UAB CFAR), P30-AI-124414 (ERC-CFAR), P30-MH-116867 (Miami CHARM), UL1-TR001409 (DC CTSA), KL2-TR001432 (DC CTSA), and TL1-TR001431 (DC CTSA).

References

1. Upasani V, Rodenhuis-Zybertid I, Cantaertid T. Antibody-independent functions of B cells during viral infections. *PLoS Pathog*. 2021;17(7):e1009708.

2. Gerlich WH. Prophylactic vaccination against hepatitis B: achievements, challenges and perspectives. *Med Microbiol Immunol*. 2015;204(1):39–55.

3. T Jake L. Hepatitis B: The Virus and Disease. *Hepatology*. 2009;49:S13–S21.

4. Loomba R, Liang TJ. Hepatitis B Reactivation Associated With Immune Suppressive and Biological Modifier Therapies: Current Concepts, Management Strategies, and Future Directions. *Gastroenterology*. 2017;152(6):1297–1309.

5. Lee J, et al. Rituximab and hepatitis B reactivation in HBsAg-negative/anti-HBc-positive kidney transplant recipients. *Nephrology Dialysis Transplantation*. 2017;32(4):722–729.

6. Leandro MJ. B-cell subpopulations in humans and their differential susceptibility to depletion with anti-CD20 monoclonal antibodies. *Arthritis Res Ther*. 2013;15(Suppl 1):S3.

7. Oliviero B, et al. Enhanced B-cell differentiation and reduced proliferative capacity in chronic hepatitis C and chronic hepatitis B virus infections. *J Hepatol*. 2011;55(1):53–60.

8. Xu X, et al. Reversal of B-cell hyperactivation and functional impairment is associated with HBsAg seroconversion in chronic hepatitis B patients. *Cell Mol Immunol*. 2015;12(3):309–316.

9. Burton AR, et al. Circulating and intrahepatic antiviral B cells are defective in hepatitis B. *Journal of Clinical Investigation*. 2018;128(10):4588–4603.

10. Salimzadeh L, et al. PD-1 blockade partially recovers dysfunctional virus-specific B cells in chronic hepatitis B infection. *Journal of Clinical Investigation*. 2018;128(10):4573–4587.

11. Das A, et al. IL-10-Producing Regulatory B Cells in the Pathogenesis of Chronic Hepatitis B Virus Infection. *The Journal of Immunology*. 2012;189(8):3925–3935.

12. Gong Y, et al. Role of IL-10-Producing Regulatory B Cells in Chronic Hepatitis B Virus Infection. *Dig Dis Sci*. 2015;60(5):1308–1314.

13. Le Bert N, et al. Comparative characterization of B cells specific for HBV nucleocapsid and envelope proteins in patients with chronic hepatitis B. *J Hepatol*. 2020;72(1):34–44.

14. Gu S, et al. Circulating HBsAg-specific B cells are partially rescued in chronically HBV-infected patients with functional cure. *Emerg Microbes Infect*. 2024;13(1):2409350.

15. Zhang JW, et al. Varied immune responses of HBV-specific B cells in patients undergoing pegylated interferon-alpha treatment for chronic hepatitis B. *J Hepatol*. 2024;81(6):960–970.

16. Thio CL. Hepatitis B and human immunodeficiency virus coinfection. *Hepatology*. 2009;49(S5):S138–S145.

17. Hadler SC, et al. Outcome of hepatitis B virus infection in homosexual men and its relation to prior human immunodeficiency virus infection. *Journal of Infectious Diseases*. 1991;163(3):454–459.

18. RJ B, JJ G, J H. Accelerated Loss of Antibody to Hepatitis B Surface Antigen among Immunodeficient Homosexual Men Infected with HIV. *New England Journal of Medicine*. 1987;316(10):630–631.

19. Laukamm-Josten U, et al. Decline of naturally acquired antibodies to hepatitis B surface antigen in HIV-1 infected homosexual men. *AIDS*. 1988;2(5):400–401.

20. Moir S, Fauci AS. B-cell responses to HIV infection. *Immunol Rev*. 2017;275(1):33–48.

875 21. Portugal S, et al. Atypical memory B cells in human chronic infectious diseases: An interim
876 report. *Cell Immunol*. 2017;321(July):18–25.
877 22. Cascino K, Roederer M, Liechti T. OMIP-068: High-Dimensional Characterization of Global
878 and Antigen-Specific B Cells in Chronic Infection. *Cytometry Part A*. 2020;97(10):1037–1043.
879 23. D'Souza G, et al. Characteristics of the MACS/WIHS Combined Cohort Study: Opportunities
880 for Research on Aging with HIV in the Longest US Observational Study of HIV. *Am J Epidemiol*.
881 2021;190(8):1457–1475.
882 24. Falade-Nwulia O, et al. Incident hepatitis B virus infection in HIV-infected and HIV-
883 uninfected men who have sex with men from Pre-HAART to HAART periods: A cohort study.
884 *Ann Intern Med*. 2015;163(9):673–680.
885 25. Kaslow RA, et al. The Multicenter AIDS Cohort Study: Rationale, Organization, and Selected
886 Characteristics of the Participants. *Am J Epidemiol*. 1987;126(2):310–318.
887 26. Falade-Nwulia O, et al. Outcomes of acute hepatitis B virus (HBV) in HIV infection with and
888 without HBV-active antiretroviral therapy. *AIDS*. 2021;35(6):991–993.
889 27. Liechti T, et al. An updated guide for the perplexed: cytometry in the high-dimensional era.
890 *Nat Immunol*. 2021;22:1190–197.
891 28. Van Gassen S, et al. FlowSOM: Using self-organizing maps for visualization and
892 interpretation of cytometry data. *Cytometry Part A*. 2015;87(7):636–645.
893 29. Kleberg L, et al. Regulation of B-cell function and expression of CD11c, T-bet, and FcRL5 in
894 response to different activation signals. *Eur J Immunol*. 2024;54:2350736.

30. Blair PA, et al. CD19+CD24hiCD38hi B Cells Exhibit Regulatory Capacity in Healthy Individuals but Are Functionally Impaired in Systemic Lupus Erythematosus Patients. *Immunity*. 2010;32(1):129–140.

31. Moir S, et al. Evidence for HIV-associated B cell exhaustion in a dysfunctional memory B cell compartment in HIV-infected viremic individuals. *J Exp Med*. 2008;205(8):1797–1805.

32. Amu S, et al. Frequency and phenotype of B cell subpopulations in young and aged HIV-1 infected patients receiving ART. *Retrovirology*. 2014;11(1).

33. Liechti T, et al. Widespread B cell perturbations in HIV-1 infection afflict naive and marginal zone B cells. *Journal of Experimental Medicine*. 2019;216(9):2071–2090.

34. Reiss G, Keeffe EB. Review article: hepatitis vaccination in patients with chronic liver disease. *Aliment Pharmacol Ther*. 2004;19(7):715–727.

35. Yip TCF, et al. Current and Past Infections of HBV Do Not Increase Mortality in Patients With COVID-19. *Hepatology*. 2021;74(4):1750–1765.

36. Müller G, Höpken UE, Lipp M. The impact of CCR7 and CXCR5 on lymphoid organ development and systemic immunity. *Immunol Rev*. 2003;195:117–135.

37. Malaspina A, et al. Appearance of immature transitional B cells in HIV-infected individuals with advanced disease: correlation with increased IL-7. *PNAS*. 2006;103(7):2262–2267.

38. Lemoine S, et al. Human T cells induce their own regulation through activation of B cells. *J Autoimmun*. 2011;36(3–4):228–238.

39. Sarvaria A, et al. IL-10+ regulatory B cells are enriched in cord blood and may protect against cGVHD after cord blood transplantation. *Blood*. 2016;128(10):1346–1361.

916 40. Simon Q, et al. In-depth characterization of CD24highCD38high transitional human B cells
917 reveals different regulatory profiles. *Journal of Allergy and Clinical Immunology*.
918 2016;137(5):1577-1584.e10.
919 41. Bertoletti A, Ferrari C. Adaptive immunity in HBV infection. *J Hepatol*. 2016;64(1):S71–S83.
920 42. Walker B, McMichael A. The T-cell response to HIV. *Cold Spring Harb Perspect Med*.
921 2012;2(11).
922 43. Jeannin P, et al. Human Effector Memory T Cells Express CD86: A Functional Role in Naive T
923 Cell Priming. *The Journal of Immunology*. 1999;162(4):2044–2048.
924 44. Collins M, Ling V, Carreno BM. The B7 family of immune-regulatory ligands. *Genome Biol*.
925 2005;6(6):1–7.
926 45. Knox JJ, et al. T-bet+ B cells are induced by human viral infections and dominate the HIV
927 gp140 response. *JCI Insight*. 2017;2(8).
928 46. Knox JJ, Kaplan DE, Betts MR. T-bet-expressing B cells during HIV and HCV infections. *Cell*
929 *Immunol*. 2017;321:26–34.
930 47. Sutton HJ, et al. Atypical B cells are part of an alternative lineage of B cells that participates
931 in responses to vaccination and infection in humans. *Cell Rep*. 2021;34(6).
932 48. Pape KA, et al. High-affinity memory B cells induced by SARS-CoV-2 infection produce more
933 plasmablasts and atypical memory B cells than those primed by mRNA vaccines. *Cell Rep*.
934 2021;37(2).
935 49. Meffre E, et al. Maturational characteristics of HIV-specific antibodies in viremic individuals.
936 *JCI Insight*. 2016;1(3):84610.

50. Austin JW, et al. Overexpression of T-bet in HIV infection is associated with accumulation of B cells outside germinal centers and poor affinity maturation. *Sci Transl Med*. 2019;11:eaax0904.

51. Poonia B, et al. HBV induces inhibitory FcRL receptor on B cells and dysregulates B cell-T follicular helper cell axis. *Sci Rep*. 2018;8(1).

52. Singh KP, et al. HIV-hepatitis B virus coinfection: Epidemiology, pathogenesis, and treatment. *AIDS*. 2017;31(15):2035–2052.

53. Loke RHT, et al. Diminished response to recombinant hepatitis B vaccine in homosexual men with HIV antibody: An indicator of poor prognosis. *J Med Virol*. 1990;31(2):109–111.

54. Preechanukul J, et al. Stem-like CD8+ T cells preserve HBV-specific responses in HBV/HIV co-infection. *medRxiv*. 2025.

55. Zurbuchen Y, et al. Human memory B cells show plasticity and adopt multiple fates upon recall response to SARS-CoV-2. *Nat Immunol*. 2023;24(6):955–965.

56. Pušnik J, et al. Persistent Maintenance of Intermediate Memory B Cells Following SARS-CoV-2 Infection and Vaccination Recall Response. *J Virol*. 2022;96(15).

57. Yang R, et al. The sex differences in diseases progression and prognosis among persons with HIV and HBV coinfection. *Sci Rep*. 2025;15(1).

58. Nevola R, et al. Gender Differences in the Pathogenesis and Risk Factors of Hepatocellular Carcinoma. *Biology (Basel)*. 2023;12(7).

59. Liechti T, et al. A robust pipeline for high-content, high-throughput immunophenotyping reveals age- and genetics-dependent changes in blood leukocytes. *Cell Reports Methods*. 2023;3(10).

60. Beddall M, et al. A simple tube adapter to expedite and automate thawing of viably frozen cells. *J Immunol Methods*. 2016;439.

61. Tharinger H, et al. Antibody-dependent and antibody-independent uptake of HBsAg across human leucocyte subsets is similar between individuals with chronic hepatitis B virus infection and healthy donors. *J Viral Hepat*. 2017;24:506–513.

62. Perfetto SP, et al. Quality assurance for polychromatic flow cytometry using a suite of calibration beads. *Nat Protoc*. 2012;7(12):2067–2079.

63. Parks DR, et al. Evaluating flow cytometer performance with weighted quadratic least squares analysis of LED and multi-level bead data. *Cytometry Part A*. 2017;91(3):232–249.

64. Monaco G, et al. FlowAI: Automatic and interactive anomaly discerning tools for flow cytometry data. *Bioinformatics*. 2016;32(16):2473–2480.

65. Van Gassen S, et al. CytoNorm: A Normalization Algorithm for Cytometry Data. *Cytometry Part A*. 2020;97(3):268–278.

66. Quintelier KLA, et al. CytoNorm 2.0: A flexible normalization framework for cytometry data without requiring dedicated controls. *Cytometry Part A*. 2025;107(2):69–87.

67. Becht E, et al. Dimensionality reduction for visualizing single-cell data using UMAP. *Nat Biotechnol*. 2019;37(1):38–47.

Figures

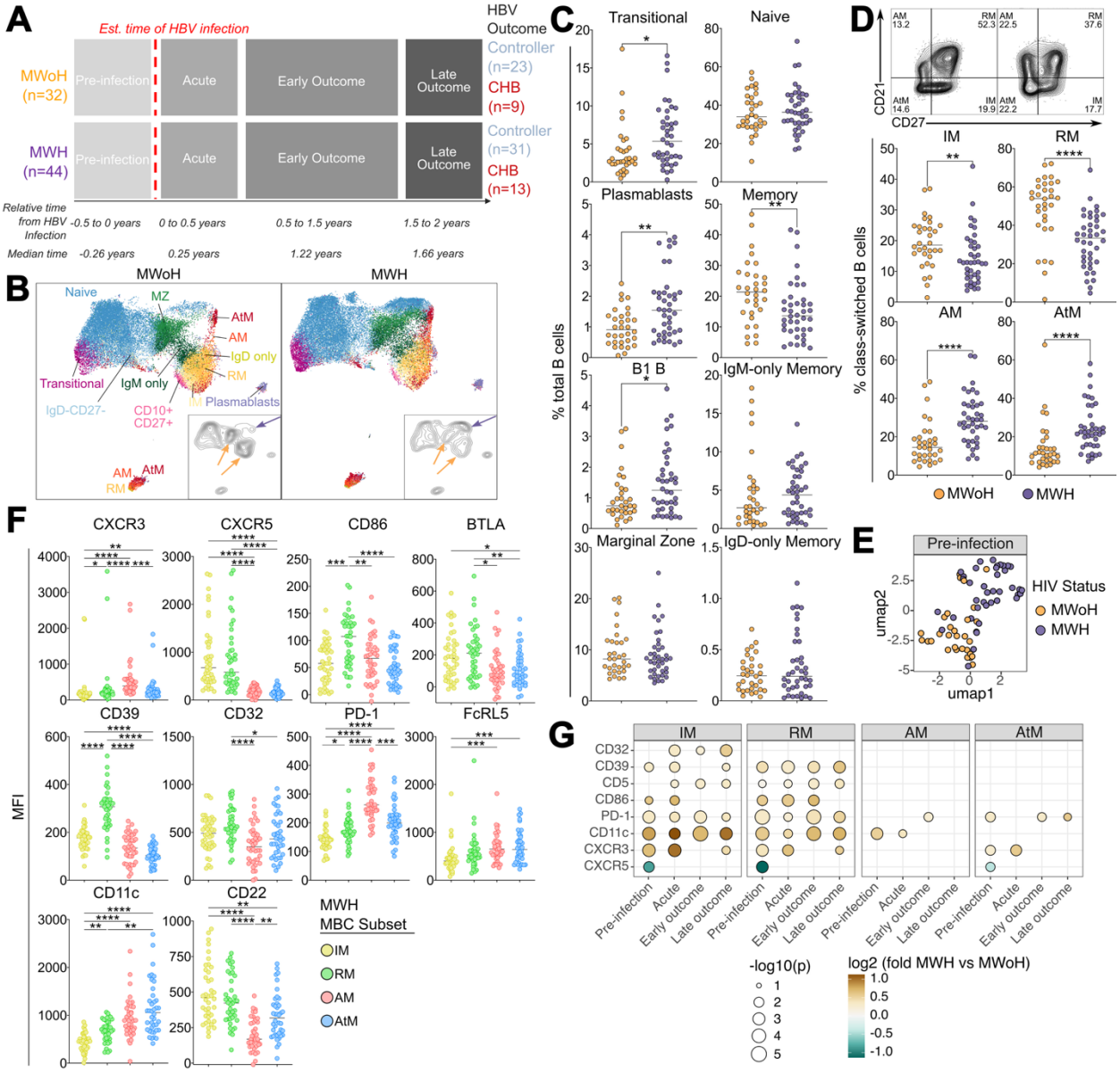

Figure 1. Global B cell subsets are significantly altered in MWH.
(A) Schematic overview of longitudinal HBV cohort. **(B)** Concatenated flow cytometry data depicted as UMAP projection of all B cells from pre-infection samples and plotted for MWoH or MWH. Each dot represents a single B cell. All markers except the dump/viability and HBsAg probes were used to compute UMAP. Contour plots depict distribution of events on UMAP based on the equally sampled pre-infection data. Yellow and purple arrows indicate areas of up- and down-regulation in MWoH and MWH, respectively. **(C)** Frequencies of B cell subsets from MWoH (orange) and MWH (purple). **(D)** Representative MWoH participant (left plot) and MWH (right plot) from the pre-infection time point were examined for expression of MBC subset markers CD27 and CD21. Frequencies of MBC subsets from all MWoH and MWH are shown below. **(E)** UMAP projection based on the composition of all B cells shown in C and D. Each dot

represents one subject at pre-infection time point. **(F)** Mean fluorescence intensity (MFI) of all phenotypic markers on MBC subsets based on CD21/CD27 expression profile from MWH pre-HBV infection. **(G)** Bubble plot highlights p-values of all significant phenotypic marker expression (MFI) on MBCs between MWoH and MWH when compared using Wilcoxon signed-rank test. Dot size is based on -log10 transformed and unadjusted p-values and dot color is based on log2 transformed (upregulated in MWH, brown; MWoH, blue) fold change. **(B-F)** Data from pre-infection samples for MWoH (n=32) and MWH (n=44). **(C-D)** Data compared using Mann-Whitney test and **(F)** Kruskal-Wallis test corrected for multiple comparisons, each dot represents a single measurement from each subject assessed at the pre-infection time point. Bars represent median values. *, $P < 0.05$; **, $P < 0.01$; ***, $P < 0.001$; ****, $P < 0.0001$.

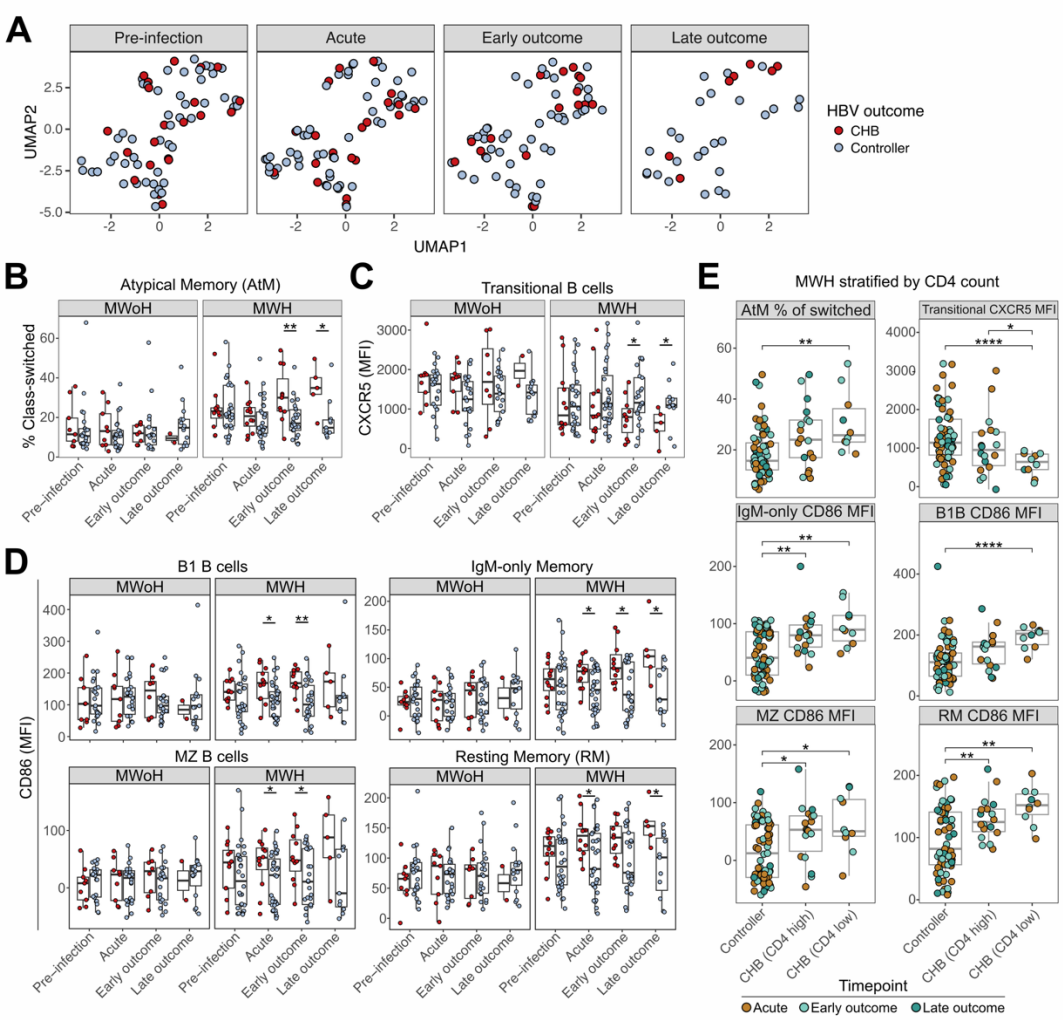

Figure 2. Differences by HBV outcome in global B cell populations are minimal and observed only in HIV-1 co-infection.

(A) UMAP projection of B cells shown in Figure 1, C and D from all MWoH and MWH at each time point (CHB, red; controller, blue). At each time point, each participant is represented by one dot. **(B-D)** Abundance of AtM (% class-switched), and expression (MFI) of CXCR5 (transitional B cells) and CD86 (B1B, IgM-only Memory, MZ and RM B cells) between HBV outcome in MWH and MWoH are shown. At each time point, each participant is represented by one dot (MWoH: pre-infection, controller n=23, CHB n=9; acute, controller n=22, CHB n=9; early outcome, controller n=21; CHB n=8; late outcome, controller n=15, CHB n=2; MWH: pre-infection, controller n=28, CHB n=12; acute, controller n=31, CHB n=12; early outcome, controller n=25; CHB n=11; late outcome, controller n=11, CHB n=5). Boxplots show median, quartile and minimum/maximum. Data compared using Wilcoxon signed-rank test. P-values are unadjusted for multiple comparisons. **(E)** Manually gated B cell characteristics compared between MWH controllers, MWH CHB with low (<350 cells/mL) and high (>350 cells/mL) CD4 counts using a GEE regression model. Each dot represents one sample, colored by time point (orange, acute; light green, early outcome; dark green, late outcome). p-values were obtained from the GEE model. *, P < 0.05; **, P < 0.01; ****, P < 0.0001.

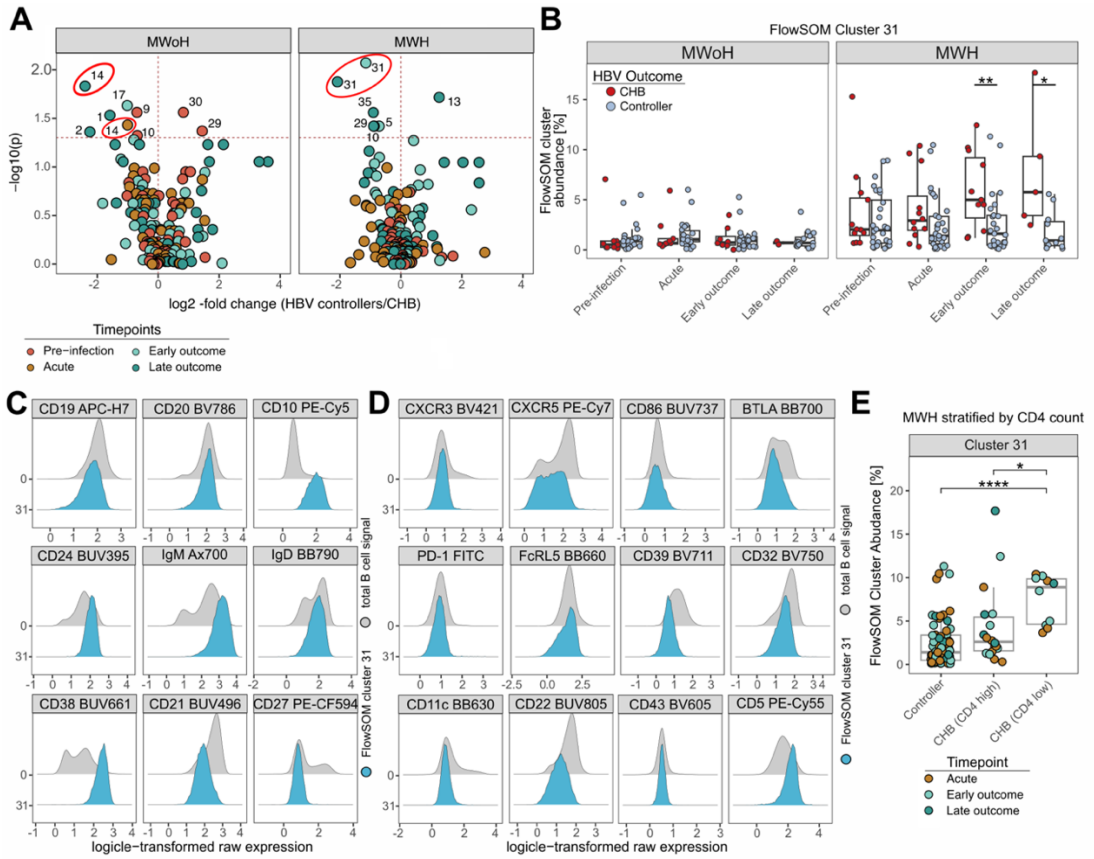

Figure 3. Unsupervised FlowSOM clustering reveals a B_{reg} population upregulated in MWH who develop CHB.

(A) Comparison of FlowSOM cluster abundance by HBV outcome in MWoH and MWH by Wilcoxon signed-rank test is shown. Volcano plot depicts -log10 transformed unadjusted p-values and log2 fold-change of cluster abundance in controllers compared to CHB. Upper right quadrant depicts clusters significantly upregulated in controllers while upper left quadrant depicts clusters significantly upregulated in CHB. Each dot represents a FlowSOM cluster colored by time point (red, pre-infection; orange, acute; light green, early outcome; dark green, late outcome). **(B)** FlowSOM cluster 31 abundance in MWoH and MWH stratified by HBV outcome is shown. Each dot represents one sample for each participant at given time point (see Figure 2 legend for sample numbers). Boxplots show median, quartile and minimum/maximum. Data compared using Wilcoxon signed-rank test. P-values are unadjusted for multiple comparisons. **(C-D)** Histogram plots show expression of all lineage markers **(C)** and phenotypic markers **(D)** for total B cells (grey) compared with FlowSOM cluster 31 (blue). **(E)** FlowSOM cluster 31 abundance compared between MWH controllers, MWH CHB with high CD4 counts (>350 cells/mL) and MWH CHB with low CD4 counts (<350 cells/mL) using a GEE regression model. Each dot represents one sample, colored by time point. p-values were obtained from the GEE model. *, P < 0.05; **, P < 0.01; ****, P < 0.0001.

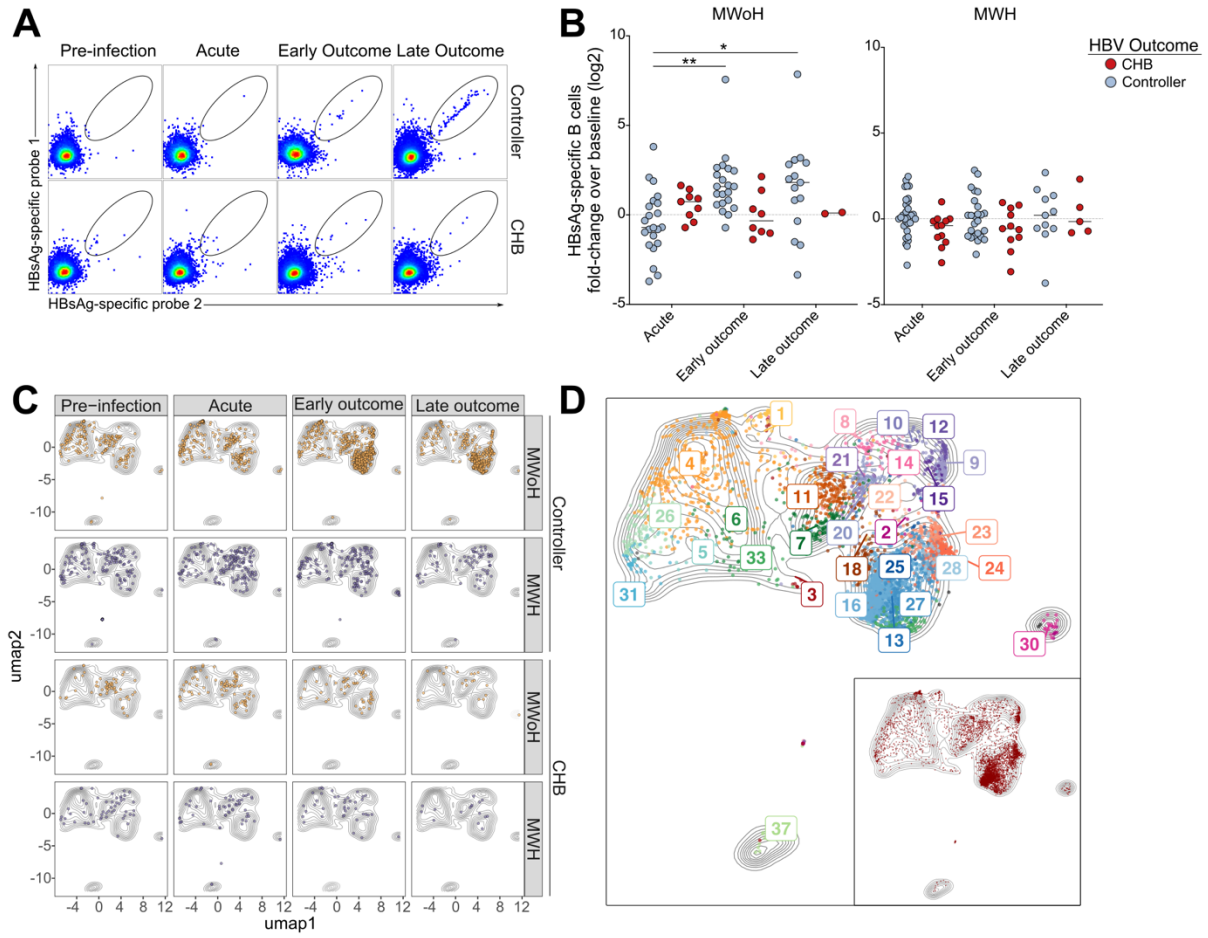

Figure 4. HBsAg-specific B cells are expanded in MWoH upon control of acute HBV infection.

(A) Flow cytometry plots of manually gated HBsAg-specific B cells from two representative participants are depicted (MWoH controller, top row; MWoH CHB, bottom row). Dual staining strategy with HBsAg probes was used to define antigen-specific B cells. **(B)** Frequencies of HBsAg-specific B cells plotted as log2 fold change over baseline. Data compared using Kruskal-Wallis test corrected for multiple comparisons. Each dot represents one participant's sample compared to baseline for each given time point (see Figure 2 legend for sample numbers). Bars represent median values. *, P < 0.05; **, P < 0.01. **(C)** UMAP projection of total B cells (contour plot, grey) overlaid with HBsAg-specific B cells (MWoH, yellow; MWH, purple) stratified by time point in controllers (top 2 rows) and CHB (bottom 2 rows). **(D)** UMAP projection of total B cells (contour plot, grey) overlaid with total HBsAg-specific B cells colored by FlowSOM cluster. Total HBsAg-specific B cells depicted in red on UMAP inlay. **(C-D)** Each dot represents a single HBsAg-specific B cell.

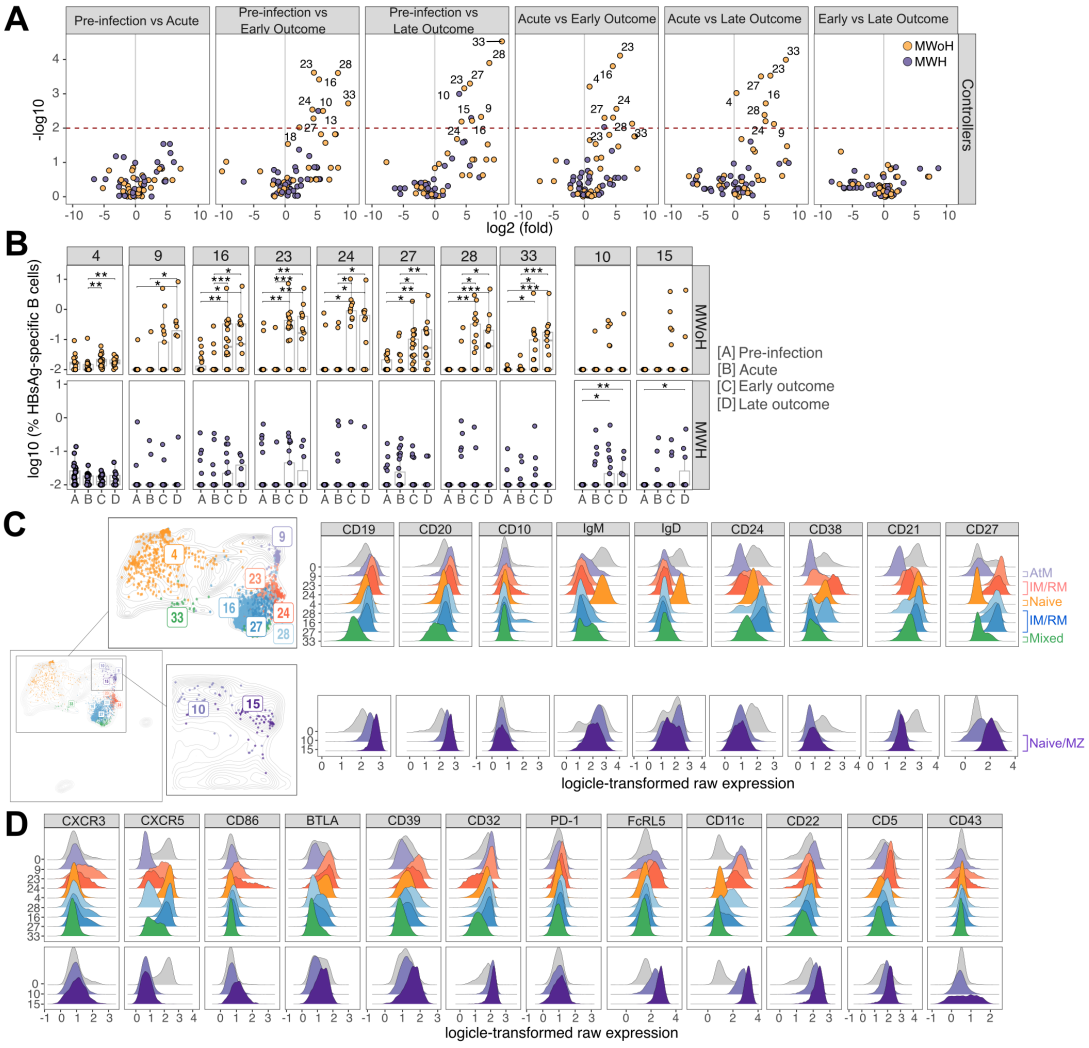

Figure 5. Expanded HBsAg-specific B cells are phenotypically heterogeneous. **(A)** Volcano plots depict log2 fold-change and -log10 transformed unadjusted p-values based on comparisons of HBsAg-specific B cell abundance by FlowSOM cluster between each possible combination of time points in HBV controllers. P-values calculated by Wilcoxon signed-rank test. Each dot represents a FlowSOM cluster, colored by HIV-1 infection status (MWoH, yellow; MWH, purple). **(B)** log10 transformed frequency of HBsAg-specific B cells over time are plotted for both MWoH and MWH controllers in 10 clusters of interest. Top row consists of clusters upregulated in MWoH; bottom row are clusters upregulated in MWH. Abundances lower than 0.01% were adjusted to 0.01% for visualization but not statistical analysis purposes. Each dot represents one sample at a given time point. Data compared by Wilcoxon signed-rank test with Bonferroni correction for multiple testing. *, P < 0.05; **, P < 0.01; ***, P < 0.001. **(C)** Previously generated UMAP of total B cells overlaid with HBsAg-specific B cells from 10 clusters of interest are colored by FlowSOM cluster. HBsAg-specific B cells are plotted on zoomed in sections of total UMAP (top row: expanded in MWoH; bottom row: expanded in MWH). **(C-D)** Histogram plots show expression levels for all lineage markers **(C)** and phenotypic markers **(D)** assessed in the panel for each of the 10 FlowSOM clusters compared with total B cells (grey histograms).

Tables

Table 1. Characteristics of incident HBV infected participants from MACS cohort.

	Men without HIV	Men with HIV
Participants (no.)	32	44
Age at estimated HBV infection (yr)	33 (20-57)	37 (21-74)
HIV VL (copies/mL)[A]	NA	18,549 (50-74,232)[B]
CD4 count (cells/mm^3)[A]	916 (362-1345)[C]	574 (160-1295)
HIV treatment (no.)[D]	NA	8
HBV Outcome (no.)		
Controller	23	31
CHB	9	13
HBV VL (IU/mL)[E]		
Controller	1.86e8 (0-2.96e9)[F]	2.58e6 (0-1.16e7)[G]
CHB	3.98e7 (1.01e7-8.74e7)[C]	1.56e8 (0-5.11e8)[I]

All MACS participants are XY male and identify as men. [A]Measured pre-HBV infection. [D]HIV treatments include: lam, tdf, lam/tdf, ftc/tdf, lam/ftc/tdf. [E]Measured in acute HBV infection. Data missing for: 26[G], 11[B], 5[F], 3[I], and 2[C] participants. Chronic HBV (CHB).

Table 2. HBV disease state serology.

	HBsAg	Anti-HBcAg	Anti-HBsAg
Controller			
Pre-infection	-	-	-
Acute			
controller 1	+	-/+	-
controller 2	-	+	+
Early Outcome	-	+	+
Late Outcome	-	+	-/+
Chronic HBV (CHB)			
Pre-infection	-	-	-
Acute	+	-/+	-
Early Outcome	+	+	-
Late Outcome	+	+	-

Plasma serology measures. Hepatitis B surface antigen (HBsAg), antibody against hepatitis B core antigen (anti-HBcAg) and antibody against HBsAg (anti-HBsAg).